

IONIC LIQUID–ELECTRODE INTERFACE: CLASSIFICATION OF IONS, SATURATION OF LAYERS, AND STRUCTURE-DETERMINED POTENTIALS

Karl Karu ¹, Eva Roos Nerut ¹, Xueran Tao ¹, Sergei A. Kislenco ², Kaija Pohako-Esko ³, Iuliia V. Voroshylova ^{4*}, Vladislav B. Ivaništšev ^{1*}

¹ Institute of Chemistry, University of Tartu, Ravila 14a, 50411 Tartu, Estonia

² Joint Institute for High Temperatures, Russian Academy of Sciences, Moscow, 125412 Russia

³ IMS Lab, Institute of Technology, University of Tartu, Nooruse 1, 50411 Tartu, Estonia

⁴ REQUIMTE LAQV, Department of Chemistry and Biochemistry, Faculty of Sciences, University of Porto, 4169-007 Porto, Portugal

* Correspondence: vladislav.ivanistsev@ut.ee, voroshylova.iuliia@fc.up.pt

Abstract

Progress in electrochemical applications of ionic liquids builds on an understanding of electrical double-layer. This computational study focuses on structure-determined quantities – maximum packing density, potentials and capacitances – evaluated using a one-electrode electrical double-layer model. Interfaces of 40 studied ions are grouped into four distinct classes according to their characteristic packing at the model surface. The simulations suggest that the exact screening by a monolayer of counter-ions (preceding the crowding of ions) is unlikely for common ions within the electrochemical stability window of corresponding ionic liquids. This work discusses how the assessed structure-determined quantities can guide the experimental tuning of (electro/mechano)chemical properties and characterising the structure of ionic liquid–electrode interfaces.

Keywords: potential of monolayer charge, maximum packing density, ionic liquids, molecular dynamics simulations, electrical double layer, overscreening, crowding, interface.

1.1. Introduction

The potential of applying ionic liquids (ILs) in technological applications motivates extensive studies of the electrical double layer (EDL) at IL–electrode interfaces [1]. Remarkable advances have been reached in the experimental characterisation of such interfaces. Namely, the unique layering of ions near the electrode surface (known as *overscreening*) was accessed with an impressively wide range of spectroscopy [2–10], microscopy [11–17], and electrochemistry [18–26] techniques. In addition to overscreening, the theoretically predicted *crowding* of counter-ions [27–30] was observed in computer simulations [31–33]. The modelled overscreening-to-crowding transition corresponds to the maximum density of ions packed in a monolayer of counter-ions [34–36], which appears in various molecular dynamics (MD), Monte Carlo, and classical density functional theory studies [37–39]. However, neither crowding nor monolayer formation has been decisively demonstrated in experiments referring to the overscreening and crowding concepts [40–48].

In a series of electrochemical experiments, Belotti *et al.* recently applied a voltage pulse and attributed the induced long-living EDL structure to a crowding regime [40]. Using atomic force microscopy, Jurado *et al.* observed a change in the EDL thickness and attributed it to the overscreening-to-crowding transition [41]. Dutta *et al.*, similarly to previously mentioned researchers, (mis)used the term “crowded” to describe the variation in X-ray reflectivity – a method that does not directly differentiate between anions and cations – actually showing that the described dense EDL is a mixture of both counter- and co-ions [42–44]. Klein *et al.* also associated the decrease in differential capacitance (measured by impedance spectroscopy) with crowding [45]. In all these studies, no structural evidence supporting crowding was provided. Nishi *et al.* applied various techniques to access the structure and quantify the absence of co-ions in the contact layer – a situation when only counter-ions are in contact with the surface – which they labelled crowding [46–48]. Similarly, in Joint density functional theory, Ma *et al.* reused the term “crowding” for the reorientation of ions in a saturated contact layer, preceding the true crowding [49]. Below, we show that such saturation corresponds to the overscreening regime. Thus, in these and similar studies, the term “crowding” is probably

misused to describe fascinating yet distinct phenomena. The question is: How to discuss new and anomalous phenomena in terms of overscreening and crowding, even when comprehensive and complementary experimental evidence is absent? The present work suggests the maximum packing density of IL ions (θ_M) and the Galvani potential of monolayer formation (φ_M) as a ballpark estimate for electrochemically measurable surface charge density (σ) and applied potentials (U vs. potential of zero charge (PZC)) for avoiding ungrounded speculations.

Previously, θ_M was evaluated for a limited set of ions in work [49,50], concluding that the monolayer of practically important ions (like Im_4^+ , TFSI^- , FEP^- ; see the [SI Table S1](#)) is unlikely to form under experimental conditions. In this work, we predicted θ_M values for a larger set of ions with different sizes and shapes (see [Figure 1](#)). This article describes how similar structure-determined quantities can guide the experimental characterisation of crowded EDL and tuning (electro/mechano)chemical properties of IL–electrode interfaces.

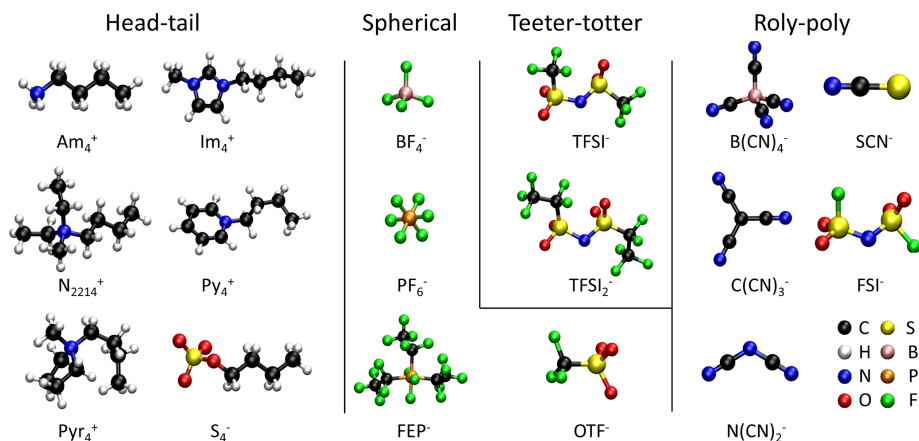


Figure 1: Ball-and-stick model of selected ions representing four identified classes. See Appendix Table 1. for names and acronyms.

1.2. Methods

1.2.1. Phenomenological model

The phenomenological ionic bilayer model simplifies the layered IL–electrode interface to two layers so that the contact layer of counter-ions overscreens the surface charge and the subsequent layer neutralises the charge excess [36]. This model defines structure-determined potentials (φ_s and φ_M) and capacitances (C_s and C_M) in terms of a scaling exponent (a), the Helmholtz capacitance (C_H), relative and vacuum permittivities

(ε and ε_0), the distance between the EDL charge density planes (l) and the maximum packing density (θ_M) as:

$$C_S = C_H \text{ and } C_M = aC_H \text{ and } C_H = \varepsilon\varepsilon_0/l \quad (1)$$

and

$$\varphi_S = \frac{\theta_M}{C_H} \left(\frac{1}{a} \right)^{\frac{1}{a-1}} \text{ and } \varphi_M = \frac{\theta_M}{C_H} \quad (2)$$

The derivation of Eqs. 1 and 2, along with a description of all quantities, is included in the SI. The evaluated θ_M and estimated (C_M, φ_M) and (C_S, φ_S) values for 40 ions are presented below in Tables 1–3. φ_M is the potential at which the monolayer of counter-ions exactly screens the surface charge ($\sigma = -\theta_M$). φ_S is the potential at which the contact layer becomes saturated with counter-ions. In between φ_S and φ_M , the prevailing mechanism of surface charge screening is the desorption of the co-ions from the second layer. This mechanism leads to a decrease in differential capacitance. C_S and C_M are the differential capacitance values at φ_S and φ_M . In this model, the distance of the closest approach gives the Helmholtz capacitance (C_H).

1.2.2. Simulated model

The EDL in ILs is commonly simulated using a two-electrode model with IL confined between electrodes [51,52]. The two-electrode model allows for keeping constant surface charge, potential difference, or applied field in the simulations [53–55]. The bisection of a two-electrode model gives a one-electrode EDL model that is commonly applied in electrocatalysis simulations [56]. [Figure 2](#) illustrates charging regimes, structures, and mechanisms showing only a minimal number of counter- and co-ions that screen the surface charge in both models (see Refs. [28,35] for details).

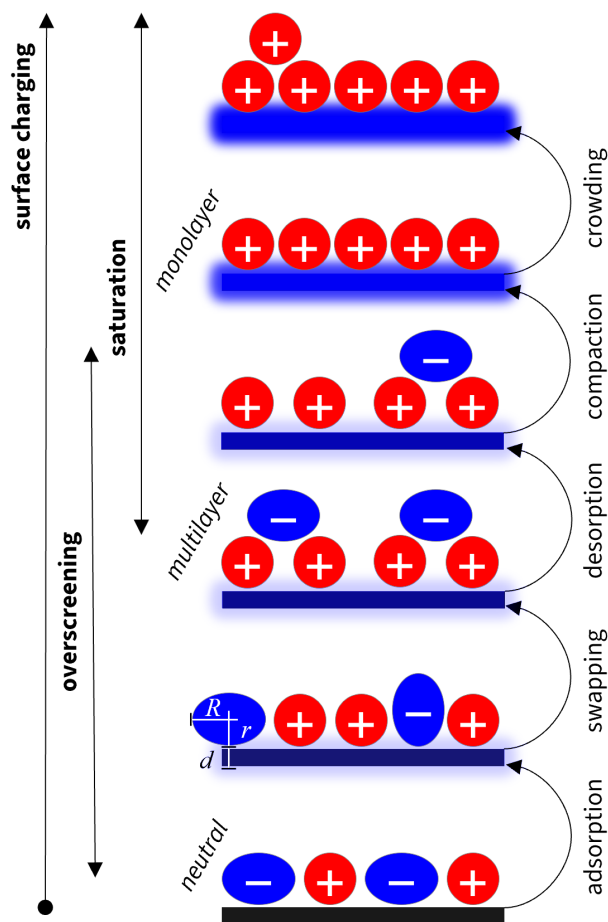


Figure 2: Schematic representation of an ionic liquid–electrode interface at variable surface charge density that is screened by shown counter- and co-ions. Processes of surface charging, overscreening, and saturation are highlighted with bold on the left. Charging mechanisms are marked on the right. Neutral, multilayer, and monolayer structures are labelled in italics. Parameters d , r , and R are shown.

This work simplifies the one-electrode EDL model to include only counter-ions, as in the Helmholtz model [57]. This model estimates the maximum packing density, assuming that θ_M is determined by the geometry of ions. Previous simulations show that when $\sigma = -\theta_M$, the monolayer of counter-ions completely screens the surface charge density [35]. On this basis, it can be assumed that the θ_M and φ_M values are similar for simulations with both one-electrode and more sophisticated two-electrode models. This assumption is valid for the packing of PF_6^- simulated in this work and Refs. [36,58] (see [Figure 3](#)) using one- and two-electrode models, respectively. Herewith, the simplified

one-electrode model shortens the simulation time by two orders of magnitude compared to the two-electrode model.

1.2.3. *Molecular dynamics simulations*

The simulations were performed with the GROMACS 2020 software [58–64] and OPLS-AA force fields with $\pm 1e$ charges on ions [65–67]. The graphene-like electrode was prepared using the Atomic Simulation Environment [68] with a size of 4.26 nm \times 3.94 nm (640 carbon atoms) and a 0.30 nm tolerance for packing. The Packmol software [69] generated five replicas with different packing for a variable number of counter-ions.

First, a rough energy minimisation run was performed with a steepest descent method with 0.01 nm step size and 10 kJ mol⁻¹ nm⁻¹ force convergence threshold. Then, an equilibration step was run for 20 ps with 0.5 fs timestep, generating velocities corresponding to the temperature of 100 K. The production run was done in the Canonical ensemble (*NVT*) for 1000 ps with 1 fs time step and velocities corresponding to 353 K. The Verlet cut-off scheme was employed, and *xy*-periodic boundary conditions were applied with the particle-mesh Ewald and 3dc Ewald correction [70–72]. Next, the trajectories were analysed. Charge and mass density profiles, as well as electrostatic potential profiles, were obtained using GROMACS tools and processed using Python scripts. MDanalysis software was used to analyse the distances [73,74]. VMD software [75] was employed for visualisation.

1.2.4. *Density functional theory calculations*

Density functional theory calculations were performed to estimate the reduction and oxidation potentials of the IL ions. The calculations were performed using the r²SCAN-3c method [76] as implemented in the Orca 5.0.2 quantum chemistry program package [77]. The r²SCAN-3c is a composite method based on a meta-generalized-gradient approximation density functional [78,79], which employs a custom triple-zeta Gaussian basis set [76], D4 dispersion correction [80,81], and geometrical counterpoise correction [82]. The SCAN functional demonstrated great accuracy for determining the energetic parameters of IL ions, especially when paired with dispersion and counterpoise corrections. [83]

The geometries of the ions were optimised using nominal charges of +1e for cations and −1e for anions. Furthermore, single-point calculations were performed to calculate the ionisation potential (IP) and electron affinity (EA) using these geometries with ionic charges of 0e and +2e for cations and −2e and 0e for anions. Under the assumption that oxidation and reduction occur adiabatically and are not affected by the environment, the IL electrochemical window for each anion–cation combination was estimated as

$$EW = \min(IP) + \max(EA), \quad (3)$$

where the EA is defined as the energy released upon accepting one electron.

1.2.5. Workflows

The NaRIBaS (Nanomaterials and Room-temperature ILs in Bulk and Slab) scripting framework was employed to construct flexible and automatic workflows [64]. The scripts with the topology files and input parameters are available at Git-Hub [84,85].

1.2.6. Structure-determined packing density, potential drops, and capacitances

The contact layer density (θ) was extracted from number density profiles using the numerical evaluation of the density slices. Moving from the electrode to the opposing end of the simulation box, the beginning of the contact layer was defined as a point where the density in a slice exceeds an ion-specific threshold. The density of a contact layer was found by integrating the density of the slices in between. [Figure 3](#) illustrates that the maximum packing density (θ_M) value corresponds to the plateau at $|\theta|$ vs. $|\sigma|$ plot. The results were visually checked with VMD software for the crowding condition.

[Figure 3](#) also shows the agreement between θ_M estimation procedures using the one- and two-electrode models [36,58]. Note that θ_M is reached at lower σ values in the two-electrode simulations. First, this is due to the presence of co-ions after the contact layer of counter-ions, *i.e.* overscreening. Second, the inflexion point corresponds to the saturation potential (φ_s), after which the prevailing mechanism of the surface charge screening is the desorption of co-ions from the EDL. Most importantly, this study shows

that in both procedures, the exact screening (by the monolayer of counter-ions) is reached when $\sigma = -\theta_M$.

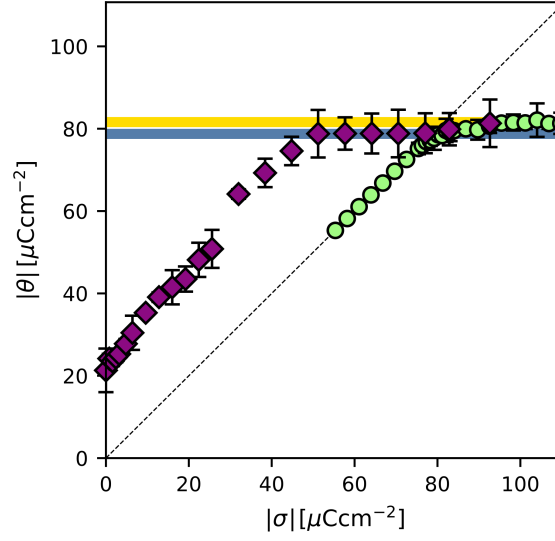


Figure 3: Contact layer charge density (θ) dependence on the surface charge density (σ) for PF_6^- . The maximum packing density (θ_M) corresponds to the plateau. The number of PF_6^- ions in the contact layer is shown with circles and diamonds for simulations with one and two electrodes, respectively. Data for the two-electrode model is from Refs. [36,58].

The monolayer potential drop ($\varphi_{M,P}$) was calculated using the Poisson equation and the charge density profiles at estimated θ_M . Then, these $\varphi_{M,P}$ values were recalculated under two assumptions: first, the partial charge transfer can be accounted for by varying relative permittivity (ϵ_r); second, the total potential drop can be split into electrode and electrolyte contributions.

The first assumption views the partial charge transfer as an extreme of electronic polarisation in the EDL. ϵ_r values from 1.6 to 2 are commonly used in MD simulations to account for electronic polarisation through atomic charge scaling as $q = \epsilon_r^{-1/2}$ [59]. In these simulations, $\epsilon_r = 1$ was used and then rescaled during analysis.

The second assumption was tested by comparing φ_M values evaluated directly *via* the Poisson equation ($\varphi_{M,P}$) and using simulated θ_M in the following expression with $q = \pm 1$ and $\epsilon_r = 1$:

$$\varphi_{M,P} = -\frac{d+r}{\epsilon_r \epsilon_0} \theta_M = -\frac{d\theta_M}{\epsilon_r \epsilon_0} + \frac{r}{R} \cdot \frac{q}{\epsilon_r \epsilon_0} \sqrt{\frac{\theta_M}{4q}} \quad (4)$$

where d is the surface atom's radius, q is the counter-ion charge ($\pm 1e$ in this study), r/R is the compression factor of an ion, *i. e.* the ratio between contact (r) and lateral (R) radii of the counter-ion (see [Figure 2](#)). The lateral radius was estimated as $R^2 = 1/4 \cdot q/\theta_M$. The compression factor indicates the degree of deviation of the ion's elliptic shape from a spherical form. The sum of d and r assumes that the distance between the surface and the contact layer is determined by the radii of surface atoms and counter-ions. This assumption is supported by the high coefficients of determination (R^2) of 0.987 for linear regression of $\varphi_{M,P}$ values (see [SI Figure S1](#)). Indeed, the potential drop within distance d from the electrode can be associated with the electrode and corrected as described in Ref. [58]. So, d is set to 0 nm in Eq. (4) under the assumption that the surface charge plane of an ideal metal electrode extends by one-half of an interplanar spacing as follows from theory [60,61] and calculations [62,63]. The φ_M-C_M and φ_S-C_S pair values given below are calculated from θ_M and r values using Eqs. 1–2 with $l = r$, $d = 0$, and $\epsilon_r = 1.6$. These parameters provide a lower estimate for the φ_M-C_M and φ_S-C_S pair values.

1.3. Results

1.3.1. Taxonomy of counter-ions

The examined ions were grouped into four classes according to their packing features: ball, head-tail, roly-poly, and teeter-totter. The $-\theta(\sigma)$ dependence differentiated the interfacial behaviour, as in [Figure 3](#). The ball and teeter-totter ions give a simple $|\theta|-\sigma$ plot with two clear intersecting lines, while head-tail and roly-poly ions give more complex $|\theta|-\sigma$ plots due to the reorientation of individual ions.

1.3.2. Ball class

As the name suggests, the ball class includes spherical ions such as BF_4^- , Br^- , Cl^- , FEP^- , I^- , OTF^- and PF_6^- . Their main packing feature is that they behave like coarse-grained spheres during the simulations and form close-packed structures.

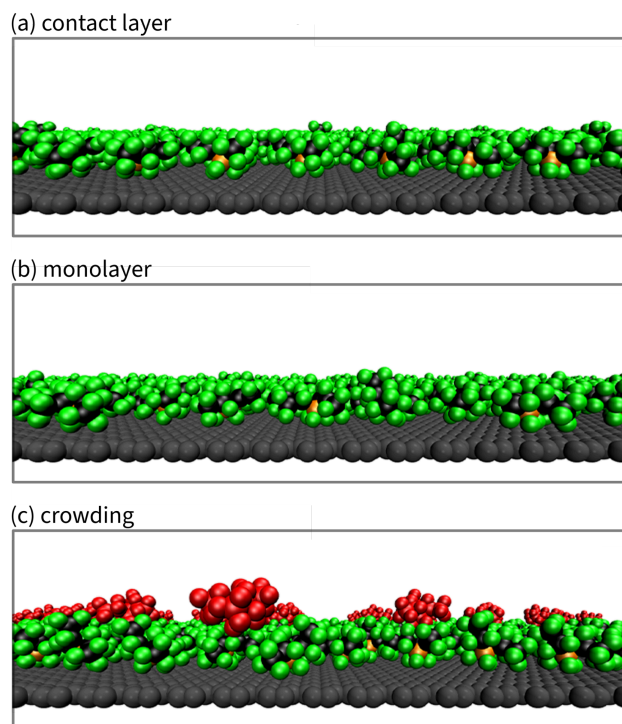


Figure 4: Side view on the ball-and-stick models of the FEP^- | electrode interface. The contact layer (a) and the monolayer (b) are visually indistinguishable, yet the crowding state (c) stands out due to ions in the second layer (shown in red).

[Figure 4](#) shows the packing of ball FEP^- ions. Due to the simple shape, ions are well organised and fill the surface in a highly ordered manner, resulting in dense packing. Ions in this class do not change orientations upon increasing $|\sigma|$. Thus, the contact layer looks indistinguishable from the monolayer (compare [Figure 4a](#) and [Figure 4b](#)) and is distinct from the crowded double layer (see [Figure 4c](#)). In the crowding regime, the projection of two ionic layers resembles a Moiré pattern (see [Figure 5a](#)), like in simulations of coarse-grained ionic liquids in Ref. [34]. Moreover, a characterization structural transition is a stepwise increase of θ with increasing $|\sigma|$. In [Figure 5](#), θ increases sharply from -150 to $-162 \mu\text{C}\cdot\text{cm}^{-2}$, which is disproportionate to the σ change of only $1 \mu\text{C}\cdot\text{cm}^{-2}$. Analogous phase transition is observed experimentally for halide anions that adsorb specifically from aqueous solutions [70]. Moreover, analogous stepwise densening was also seen in MD simulations of $\text{Au}(hkl)$ | BMImPF_6 interfaces [86].

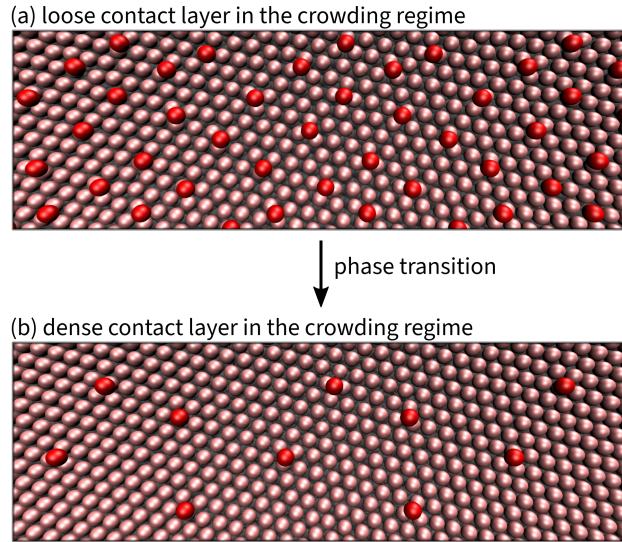


Figure 5: Top view on Br^- adlayers in the crowding regime. Ions in the first layer are shown in pink (lighter), and in the second layer, they are shown in red (darker). The phase transition from a looser contact layer (a) to a denser contact layer (b) occurs upon adding a single Br^- anion to the model unit cell.

[Table 1](#) summarises the simulated and estimated parameters of the modelled IL–electrode interfaces with ball ions. This data is discussed below. Note that in the case of PF_6^- and FEP^- the scaling exponent (a) is close to its geometrical value of 0.38 for packing of balls [36].

Table 1: Structure-determined parameters of the modelled EDLs with ball ions. The standard deviation, indicated in brackets, is computed based on the variation observed across multiple replicates.

Ion	$\theta_M [\mu\text{C}\cdot\text{cm}^{-2}]$	$\varphi_M [\text{V}]$	$\varphi_S [\text{V}]$	$C_M [\mu\text{F}\cdot\text{cm}^{-2}]$	$C_S [\mu\text{F}\cdot\text{cm}^{-2}]$	a
BF_4^-	-105.2(8)	8.3	1.5	3.9	12.6	0.31
Br^-	-149.9(7)	7.6	1.2	5.1	19.7	0.26
Cl^-	-181.3(25)	7.7	1.2	5.5	23.6	0.23
FEP^-	-25.8	7.7	1.2	5.5	23.6	0.37
I^-	-87.8(19)	6.0	1.0	3.8	14.8	0.26
OTF^-	-73.3(15)	6.2	0.9	2.8	11.8	0.23
PF_6^-	-77.5(4)	8.5	1.7	3.2	9.1	0.35

1.3.3. Head-tail class

Head-tail ions consist of an alkyl chain tail and a head, holding the ionic charge. For Py_n^+ and Im_n^+ the head is an aromatic cycle. For Am_n^+ , Pyr_n^- and N_{2214}^+ ions, the head is an (alkyl)ammonium group.

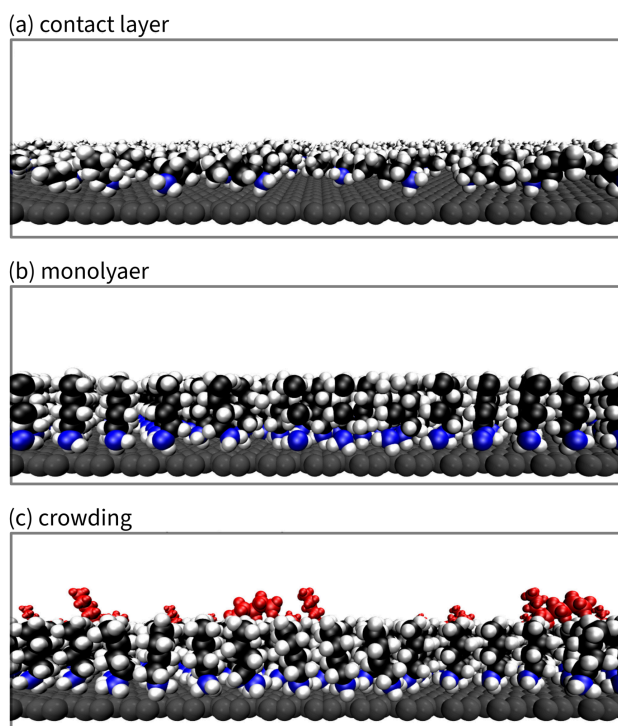


Figure 6: Side view on the ball-and-stick models of the $\text{Am}_4^+ |$ electrode interface. The maximum packing density is reached in simulations of 103 Am_4^+ ions per electrode area. Ions of the second layer are shown in red.

[Figure 6](#) shows layers of head-tail Am_4^+ ions. While at low $|\sigma|$, with enough voids on the surface, Am_4^+ tails lie parallel to the surface ([Figure 6a](#)), at high $|\sigma|$, Am_4^+ tails are forced to “stand up”, *i. e.* point outwards the surface to free void and facilitate surface charge screening by Am_4^+ heads ([Figure 6b](#)). A similar phenomenon was described in detail from MD simulations of EDLs with N_{1114}^+ , N_{1144}^+ , N_{1444}^+ , and N_{4444}^+ ions [48]. In the monolayer, all Am_4^+ tails are oriented outwards from the surface. Similar pictures are seen for all studied head-tail ions: first, in the overscreening regime, their tails can reorient; second, before and in the crowding regime, the EDL structure depends on the head-tail form and size. Five scenarios can be outlined:

(1) **Head reorientation:** Im_n^+ and Py_n^+ ions' aromatic rings (heads) change orientation from parallel to perpendicular relative to the surface. For example, the Im_n^+ monolayer has three distinguishable orientations of the Im^+ ring: one parallel and two perpendicular to the surface (with the C^2 atom pointing towards and outwards the surface). Such orientation resembles lying, standing downwards, and standing upwards at the surface and was observed in numerous MD simulations and experimental works [72,87–90].

(2) **Head-head stacking:** Ions that do not fit their head into the contact layer occupy voids between tails beyond the contact layer heads, thus appearing as head-to-head stacking.

(3) **Head-tail intercalation:** Ions that do not fit their head into the contact layer occupy voids between tails at a distance from the contact layer heads, thus appearing to intercalate the layer of tails.

(4) **Heads over tails crowding:** Ions that do not fit their head into the contact layer situated right beyond the layer of tails. In [Figure 6c](#), such ions can not penetrate the layer of tails due to a very dense packing of Am_n^+ in the contact layer. The longer the tail, the denser the layer of tails. Thus, even if head-head stacking and head-tail intercalation are possible for ions with short tails and large heads, a larger fraction of ions crowd in the layer following the tails when the tails become longer.

(5) **Tail-tails stacking:** Such behaviour, described in “Monolayer to Bilayer Structural Transition in Confined Pyrrolidinium-Based Ionic Liquids” by Smith *et al.* [91–93], was not observed in the presented simulations. Unlike the experiments, where such transition was induced by increasing the number of carbon atoms in alkyl chains (n) from 8 to 10, the presented simulations might not reproduce that bilayer structure due to the absence of co-ions stabilising the transition.

[Table 2](#) summarises simulated and estimated parameters of the modelled EDLs with head-tail ions with a tail length of 4 carbon atoms. Additional data is given in the [SI Table S1](#). Ma *et al.* also simulated Im_4PF_6 with a two-electrode model and suggested $\theta_{\text{M}}(\text{Im}_4^+)$ of $40 \mu\text{C}\cdot\text{cm}^{-2}$ [49], which agrees well with this and [50,90] studies.

Table 2: Structure-determined parameters of the modelled EDLs with head-tail ions. Only one set is shown per each family of ions, while more detailed data can be found in the [SI Table S2](#). The standard deviation, indicated in brackets, is computed based on the variation observed across multiple replicates.

Ion	$\theta_{\text{M}} [\mu\text{C}\cdot\text{cm}^{-2}]$	$\varphi_{\text{M}} [\text{V}]$	$\varphi_{\text{S}} [\text{V}]$	$C_{\text{M}} [\mu\text{F}\cdot\text{cm}^{-2}]$	$C_{\text{S}} [\mu\text{F}\cdot\text{cm}^{-2}]$	a
AM_4^+	98.3(12)	-3.5	-1.0	16.9	28.1	0.60
IM_4^+	44.9(7)	-3.3	-0.8	6.8	13.6	0.50
Py_4^+	42.4(9)	-3.0	-0.9	9.8	14.2	0.69
Pyr_4^+	44.9(10)	-5.3	-1.6	6.0	8.4	0.71
N_{2214}^+	45.6(4)	-6.2	-1.3	2.8	7.4	0.38
S_4^-	66.4(5)	5.8	1.2	4.4	11.4	0.39

1.3.4. Roly-poly class

As the class name suggests, roly-poly ions can change individual orientation from parallel to perpendicular to the surface upon increasing $|\sigma|$. Roly-poly ions “prefer” to lie flat on the surface at low $|\sigma|$, but as $|\sigma|$ increases to a certain point, ions begin to stand up to make more void for adsorbing ions. [Figure 7a](#) shows a particular state where all ions lie parallel to the surface. Increasing $|\sigma|$ forces ions to stand up, increasing the fraction of ions oriented perpendicular to the surface. In the monolayer of roly-poly ions, parallel and perpendicular orientations coexist, see [Figure 7b](#). Moreover, roly-poly ions can orient towards and outwards the surface, *i.e.* the perpendicularly oriented SCN^- ions contact the surface with sulphur or nitrogen atoms (see [Figure 7b](#) and [Figure 7c](#)). In general, roly-poly ions are drastically different from head-tail and ball ions in terms of packing at variable $|\sigma|$ (compare [Figure 4](#), [Figure 6](#), and [Figure 7](#)).

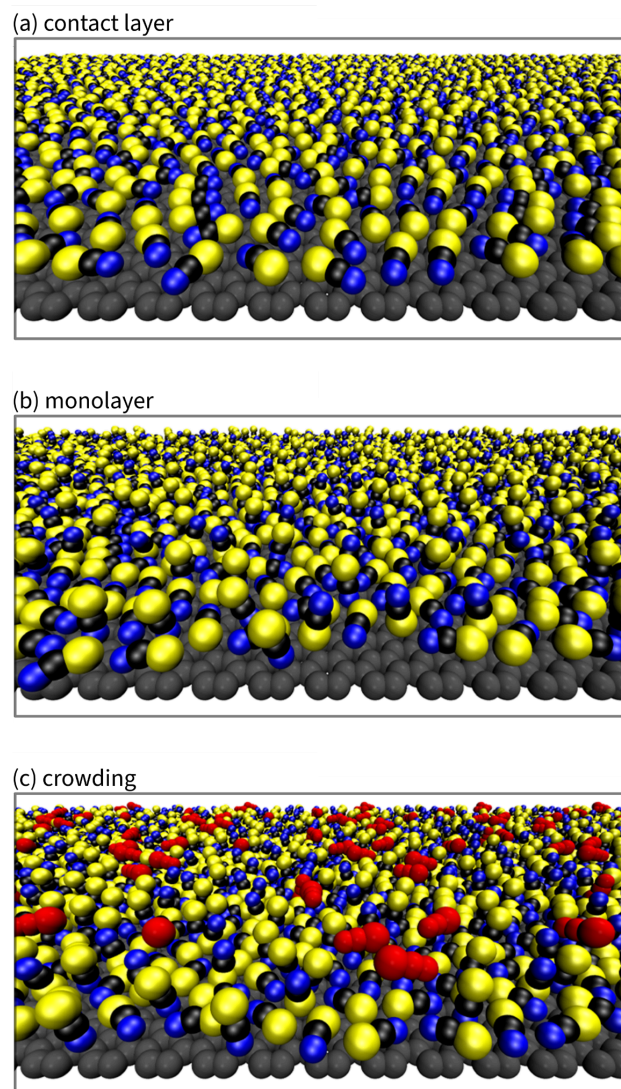


Figure 7: Side view on the ball-and-stick models of the SCN^- | electrode interface. In the low-density contact layer (a), SCN^- anions lie parallel to the surface. In the monolayer (b) and crowder state (c), a significant fraction of SCN^- ions orient perpendicular to the surface. The second layer is shown in red.

[Table 3](#) summarises the simulated and estimated parameters of the modelled EDLs with roly-poly and teeter-totter ions. This data is discussed below.

Table 3: Structure-determined parameters of the modelled EDLs with roly-poly and teeter-totter ions. The standard deviation, indicated in brackets, is computed based on the variation observed across multiple replicates.

Ion	$\theta_M [\mu\text{C}\cdot\text{cm}^{-2}]$	$\varphi_M [\text{V}]$	$\varphi_S [\text{V}]$	$C_M [\mu\text{F}\cdot\text{cm}^{-2}]$	$C_S [\mu\text{F}\cdot\text{cm}^{-2}]$	a
$\text{B}(\text{CN})_4^-$	-64.7(15)	9.1	2.4	3.8	7.1	0.53
$\text{C}(\text{CN})_3^-$	-73.7(8)	6.7	1.6	5.4	11.1	0.48
$\text{N}(\text{CN})_2^-$	-108.4(15)	7.3	1.2	3.8	14.8	0.26
SCN^-	-103.8(28)	4.1	0.5	4.5	25.3	0.18
FSI^-	-59.0(8)	5.7	1.1	3.4	10.4	0.33
PFSI^-	30.9(5)	2.8	0.6	4.9	11.1	0.44
TFSI^-	-42.2(4)	3.7	0.9	5.7	11.4	0.50

1.3.5. Teeter-totter class

The teeter-totter ions class comprises ions with a particular structure, where one central atom connects to two similar groups on both sides.

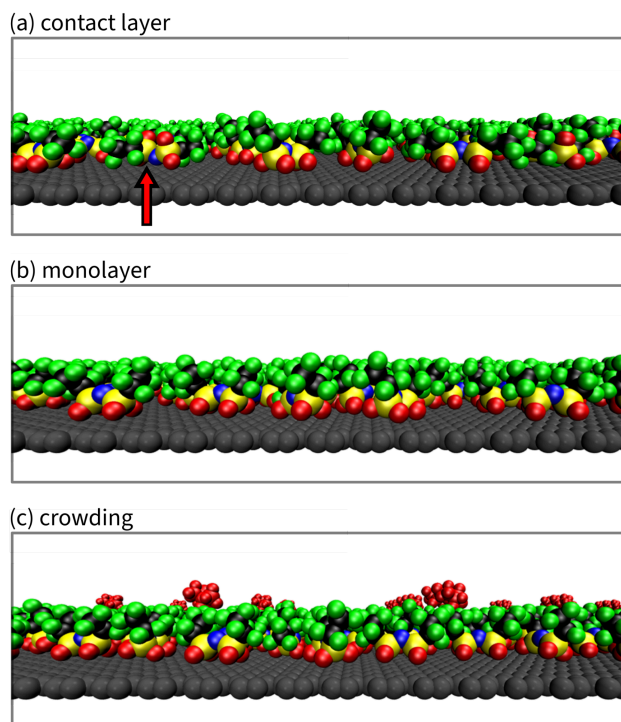


Figure 8: Side view on the ball-and-stick models of the PFSI^- | electrode interface. The contact layer (a) contains trans-conformers of PFSI^- (indicated with a red arrow), while in

the monolayer (b) all ions orient with oxygen atoms towards the surface, and in the crowding regime (c) additional ions (shown in red) form the second layer.

Although the teeter-totter ions can be considered linear and similar to the roly-poly class, they do not reorient with increasing $|\sigma|$. Only at very low $|\sigma|$, the teeter-totter ions might take a trans-configuration as marked in [Figure 8a](#) and in agreement with experimental results [47]. More negatively charged atoms of teeter-totter ions orient towards the surface at all studied $|\sigma|$.

The findings presented here align with previous MD simulations of ILs with TFSI⁻ conducted by Sharma and Kashyap [94]. In close proximity to a positively charged graphene sheet, the major axis of symmetry of the TFSI⁻ anions predominantly align parallel to the surface. This observation emphasises the significance of electrostatic interactions between oxygen atoms TFSI⁻ in and the graphene sheet, as in this study.

1.3.6. Summary of results

All evaluated $\varphi_{M,P}-\theta_M$ values along with the curve following Eq. (4) are shown in [Figure 9](#). According to the compression factor (r/R), most of the ions are ellipses (like heads of Am_n⁺ and S_n⁻ with $r/R \approx 0.4$), some ions are slightly more spherical (halide anions and Py_n⁺ with $r/R \approx 0.6$), while others are almost perfect spheres (cyano-based anions and Pyr_n⁺ with $r/R \approx 0.8$). For ball ions, [Figure 9](#) shows an obvious trend of rising φ_M value with decreasing ion radius. In a clear example of halide ions, one can see that the smaller the ion, the higher the potential of the monolayer formation. This observation is *qualitatively* in line with predictions made by Ivaništšev and Fedorov [95], where the maximum packing density was approximated by $\theta_M = 1/4 \cdot q/r^2$, taking $r = R$.

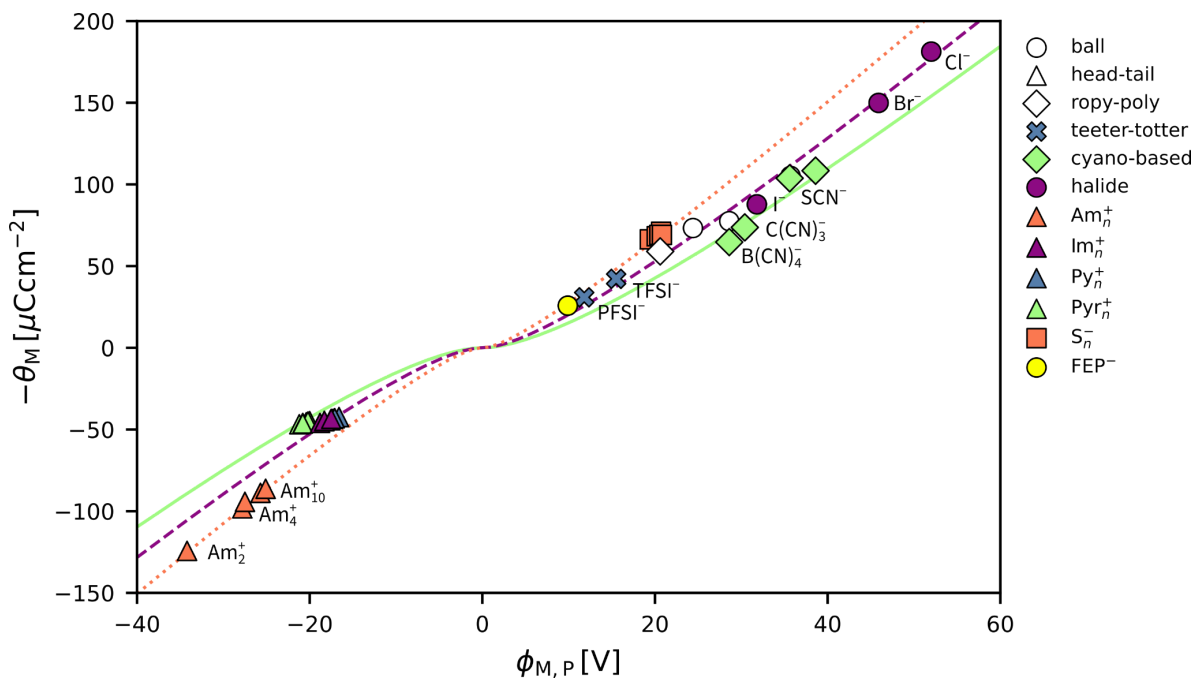


Figure 9: Calculated maximum packing density (θ_M) and monolayer potential drop ($\phi_{M,P}$) values. Lines follow Eq. (4) with compression factor (r/R) of 0.8 (solid), 0.6 (dashed), and 0.4 (dotted).

For head-tail ions, using radii from Refs. [73,74,96], Ivaništšev and Fedorov presumed a dependence of θ_M on the tail length [95]. However, in the present simulations, only θ_M of Am_n^+ depends on the tail length. Different from all simulated head-tail ions, in Am_n^+ the ammonium head and alkyl tail have similar cross-section diameters, so the stacking of tails determines the packing of heads, as can be seen in Figure 6. The lateral distance between tails increases with the number of bent conformations, *i.e.*, the tail lengthening. This effect is levelled down when the head is wider than the tail, like in Im_n^+ , Py_n^+ , and Pyr_n^+ , yielding almost the same θ_M value for these ions (see Figure 9).

2. Discussions

2.1. Comparison of structure-determined potentials

Figure 10 summarises all corrected ϕ_M - θ_M values obtained with the Poisson equation, then (1) shifting the surface charge plane by $-d\theta_M/\epsilon_0$ with $d = 0.17$ nm and (2) dividing by $\epsilon_r = 2$. The shown θ_M values correspond to the ion charge $q = \pm 1e$ as in Figure 9 and all Tables. Note that these values differ slightly from the ϕ_M values calculated using Eq. (2) and shown in Tables 1–3 and SI Table S1.

The most marked feature is that all ϕ_M values are outside the ± 2 V vs PZC region, which is the experimentally measurable potential window [50]. In other words, true monolayer formation and crowding should not be experimentally reachable for all studied ions. This conclusion holds under the assumption that the partial charge transfer is below $1 - \sqrt{1/2} = 0.3e$. The highly polarisable Py_n^+ could form the monolayer at -2 V upon accepting $0.5e$ (see [Figure 10](#)). However, the scanning tunnelling microscopy study of Py_4^+ adsorption from Py_4BF_4 did not reveal any ordered structure [97]. Halide anions could form their monolayers at $+2$ V upon donating $0.7e$. Indeed, halide anions are well known for forming highly ordered adlayers even at lower relative potentials [78,98,99]. It is worth examining whether these adlayers meet the exact screening definition by checking for evidence of overscreening and crowding. For instance, by examining the composition of the second layer with XRD and STM [100].

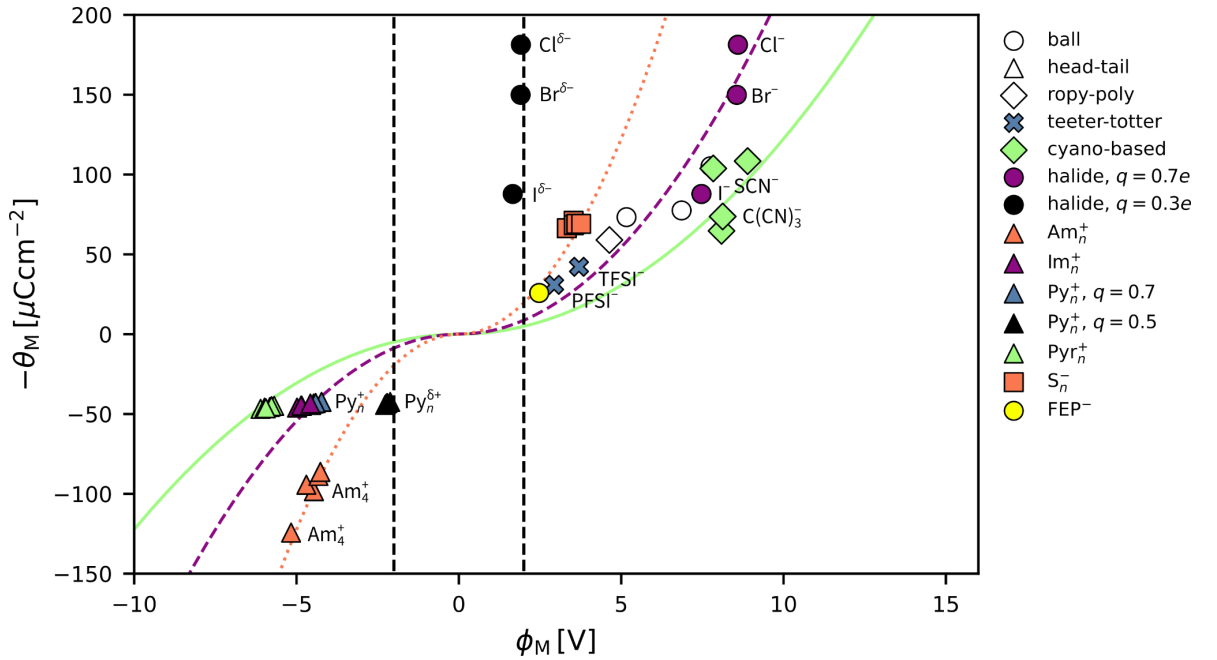


Figure 10: Simulated maximum packing density (θ_M) and recalculated monolayer potential drop (ϕ_M) values. Lines follow Eq. (4) with $d = 0$, $\epsilon_r = 2$, and compression factor (r/R) equals 0.8 (solid), 0.6 (dashed), and 0.4 (dotted).

On the contrary to ϕ_M values, the estimated ϕ_S values are within the ± 2 V region, as reported in Tables 1–3. That means most of the reported ordered adlayers [11,16,24,79–81,83,101–103] form near the saturation potential (ϕ_S). [Figure 2](#) illustrates this conclusion with results for two electrode simulations of BMImPF₆ [36,58], where ϕ_S

of 3 V was estimated for PF_6^- anions. In this work, the corresponding estimation is 2.2 V for the same ϵ_r of 1.6. Despite crude approximations in Eq. (2) for φ_s , it leads to a phenomenologically reasonable conclusion that interfacial processes attributed to crowding (e.g. Refs. [40]) are most probably occurring in the overscreening state (see Refs. [16,104]). Moreover, switching on and off applicable properties such as capacitance, lubricity, actuating property, [105–107] are probably related to the change in the screening mechanism at φ_s : from adsorption of counter-ions to desorption of co-ions from the second layer. [36,49,108]

2.2. Structure-determined potentials and the electrochemical window

A simple procedure for finding surfaces with φ_M and φ_s values within the electrochemical stability window (EW) of ionic liquid–electrode interfaces is a comparison of the lower estimate for φ_M and φ_s (Eqs. (1) and (2) with $l = r, d = 0$, and $\epsilon_r = 2$) to the upper estimate for the EW (Eq. (3)). The latter assumes that ions decompose solely *via* electron transfer neglecting the solvation. The predicted EWs vary from 4 to 12 V for four hundred anion–cation combinations. These are overestimated due to ignorance of essential aspects such as EDL structure, decomposition mechanism, catalytic effect and reactivity of the surface, and partial charge transfer, which should narrow the EW. Moreover, adjustment by the PZC should further narrow the EW because anodic and cathodic processes are interrelated through the electroneutrality principle. Summing φ_M and φ_s for anion–cation combinations cancels φ_{PZC} out. Tables 4 and 5 show the differences $\text{EW} - \Delta\varphi_M$ and $\text{EW} - \Delta\varphi_s$ for selected anion–cation ILs. The full compassion (given in the SI) provides an optimistic estimation of whether φ_M and φ_s fit into the EW.

Table 4: Difference between predicted EW and $\Delta\varphi_M$ values. Positive values imply that φ_M values might be experimentally reached.

	Br^-	Cl^-	I^-	BF_4^-	PF_6^-	$\text{N}(\text{CN})_2^-$	$\text{C}(\text{CN})_3^-$	$\text{B}(\text{CN})_4^-$	FSI^-	TFSI^-	PFSI^-	FEP^-
Pyr_4^+	-8.4	-8.5	-6.9	-5.8	-5.7	-7.7	-7.0	-6.0	-5.4	-3.4	-2.5	-0.9
AM_4^+	-5.3	-5.4	-3.7	-2.7	-2.5	-4.5	-3.9	-2.8	-2.3	-0.3	0.6	2.2
IM_4^+	-4.4	-4.5	-2.8	-1.8	-1.6	-3.6	-3.0	-1.9	-1.4	0.6	1.5	3.2
Py_4^+	-2.6	-2.7	-1.0	0.0	0.2	-1.8	-1.1	-0.1	0.4	2.4	3.3	5.0

Table 5: Difference between predicted EW and $\Delta\varphi_s$ values. Positive values imply that φ_s values might be experimentally reached.

	Br ⁻	Cl ⁻	I ⁻	BF ₄ ⁻	PF ₆ ⁻	N(CN) ₂ ⁻	C(CN) ₃ ⁻	B(CN) ₄ ⁻	FSI ⁻	TFSI ⁻	PFSI ⁻	FEP ⁻
Py ₄ ⁺	1.6	1.7	1.8	4.6	4.9	2.2	1.7	4.5	2.9	3.0	3.3	5.2
AM ₄ ⁺	3.6	3.7	3.8	6.6	6.8	4.1	3.7	6.5	4.8	5.0	5.3	7.2
IM ₄ ⁺	4.5	4.5	4.6	7.4	7.7	5.0	4.5	7.3	5.7	5.9	6.1	8.0
Py ₄ ⁺	5.9	5.9	6.0	8.9	9.1	6.4	6.0	8.7	7.1	7.3	7.5	9.5

For all studied ionic liquids the difference between anionic and cationic φ_s values ($\Delta\varphi_s$) fit into the predicted EW (Table 5). Considering the crudeness of approximations, that does not guarantee that the saturation potential is achievable within the measurable EW for all ions. Still, it is a good sign that saturation is experimentally verifiable.

An opposite conclusion applies to the possibility of fitting the monolayer potential into the EW (Table 4). The difference between anionic and cationic φ_M values ($\Delta\varphi_M$) does not fit the predicted EW for most anion–cation combinations. An exceptional cation is Py_n⁺ due to its flat geometry. As discussed above Py_n⁺ is also the most polarisable among other studied cations. However, such polarisation reduces both φ_M and the EW and, in sum, excludes monolayer formation prior to decomposition. Unlike Py_n⁺, all exceptional anions (TFSI⁻, PFSI⁻, and FEP⁻) are non-polarizable in simulations and electrochemically stable in experiments. Still, they are not as stable as predicted by Eq. (3) because of decomposition through bond breaking. Even if ILs consisting of TFSI⁻, PFSI⁻, or FEP⁻ do not form the monolayer within real EW, these as well as BF₄⁻, PF₆⁻, B(CN)₄⁻ anions are the best candidates for exploring the saturation regime at ionic liquid–electrode interfaces. However, ions of another shape should be considered to reach the monolayer formation.

2.3. Ion shape and the monolayer potential

The obtained data answers an essential question – whether monolayers of physisorbed ions are, in principle, achievable. The criteria for such a possibility is a realistically low $|\varphi_M|$ value below 2 V. For the ball ions, the potential can be translated into a radius of over 1.1 nm assuming that $\epsilon_r = 2$ and $d = 0$ in Eq. (4). In other words, hard

ball ions of $\pm 1e$ charge and 1.1 nm radius form a monolayer at ∓ 2 V. All studied and most known ILs ions have much smaller dimensions. For comparison, the highest estimated R value in this study equals 0.8 nm. An example from the literature is the polyoxometalate $\text{PW}_{12}\text{O}_{40}^{3-}$ anion with a radius of 0.55 nm. This anion was discussed by Borukhov *et al.* in Refs. [109,110] to illustrate the idea of crowding. A simple estimation of φ_M for $\text{PW}_{12}\text{O}_{40}^{3-}$ gives an unreachable potential value of +13 V!

[Figure 10](#) hints at an alternative way to lower the $|\varphi_M|$ by decreasing the compression factor. Indeed, a flat and wide frisbee-shaped cation with $r = 0.17$ nm and $R = 0.44$ nm should form a monolayer at -2 V. This is comparable to the size of 3*N*-coronene cations – one of the smallest representatives of nitrogen-substituted polycyclic aromatic hydrocarbon (PAH) cations [111]. Similar PAH could be substituted with boron [112] to provide frisbee anions. There is no record of PAH-based ILs being synthesised up to date. Yet, numerous experiments with triangulenium cations visualised ordered adlayers [113,114]. More realistic estimations at the density functional theory level predict that larger PAH ions are potential candidates for crowding at relatively small potentials [115].

2.4. Concluding remarks and future research directions

In this work, we performed classical MD simulations of the 40 most common ions (constituting ILs) on a graphene surface. Within this simple one-electrode model, we estimated the potentials of the saturated contact layer and monolayer: φ_S and φ_M .

By comparing the estimated φ_M and φ_S values to predicted and literature data, it becomes evident that the monolayer and crowded structures of studied ions are unreachable within the experimentally measurable potential window. Still, reaching the crowded regime by designing ions of specific shape can reveal new phenomena of high applied potential, as predicted and discussed in Ref. [116]. This study shows that already-known phenomena (previously attributed to crowding) are due to the saturation of non-polarisable ions, *i.e.*, the formation of ordered layers at φ_S . Herewith, polarisable ions (like halides) might form the monolayer (exactly screening the surface charge) or even crowded EDL within the stability windows of corresponding ionic liquids due to partial charge transfer. From both fundamental and application perspectives, it is

essential to study and understand the nature of adlayers formed by such polarisable as well as non-polarizable ions. The reported data sets the reference point for future studies, where theoretical φ_S and φ_M can be used as “milepost” potentials.

2.5. Funding

This work received financial support from FCT/MCTES (UIDP/50006/2020 DOI 10.54499/UIDP/50006/2020) through Portuguese national funds.

2.6. Acknowledgements

This work was supported by the Estonian Ministry of Education and Research (TK210). V.I. acknowledges the support of the Estonian Research Council (grant STP52). I.V.V. acknowledges funding from FCT/MCTES through the Portuguese national funds (LA/P/0008/2020 DOI 10.54499/LA/P/0008/2020, UIDP/50006/2020 DOI 10.54499/UIDP/50006/2020 and UIDB/50006/2020 DOI 10.54499/UIDB/50006/2020, REQUIMTE LAQV). Results were obtained using the High-Performance Computing Center of the University of Tartu.

2.8. Supporting Information.

The supporting information contains formulas and values for structure-determined potentials (φ_S and φ_M) and capacitances (C_S and C_M) in terms of a scaling exponent (a), the Helmholtz capacitance (C_H), relative and vacuum permittivities (ϵ_r and ϵ_0), the distance between the EDL charge density planes (l , splitted into atomic radii d and r) and the maximum packing density (θ_M , recalculated into radius R). Codes for reproducing data and figures are accessible at <https://github.com/vilab-tartu/NaRIBaS>.

2.8. References

- [1] D.S. Silvester, R. Jamil, S. Doblinger, Y. Zhang, R. Atkin, H. Li, Electrical Double Layer Structure in Ionic Liquids and Its Importance for Supercapacitor, Battery, Sensing, and Lubrication Applications, *J. Phys. Chem. C* 125 (2021) 13707–13720. <https://doi.org/10.1021/acs.jpcc.1c03253>.
- [2] S. Xu, S. Xing, S.-S. Pei, V. Ivaništšev, R. Lynden-Bell, S. Baldelli, Molecular Response of 1-Butyl-3-Methylimidazolium Dicyanamide Ionic Liquid at the Graphene Electrode Interface Investigated by Sum Frequency Generation Spectroscopy and Molecular Dynamics Simulations, *J. Phys. Chem. C* 119 (2015) 26009–26019. <https://doi.org/10.1021/acs.jpcc.5b08736>.
- [3] M. Mezger, R. Roth, H. Schröder, P. Reichert, D. Pontoni, H. Reichert, Solid-liquid

- interfaces of ionic liquid solutions—Interfacial layering and bulk correlations, *J. Chem. Phys.* 142 (2015) 164707. <https://doi.org/10.1063/1.4918742>.
- [4] T.A. Petach, A. Mehta, R. Marks, B. Johnson, M.F. Toney, D. Goldhaber-Gordon, Voltage-Controlled Interfacial Layering in an Ionic Liquid on SrTiO₃, *ACS Nano* 10 (2016) 4565–4569. <https://doi.org/10.1021/acsnano.6b00645>.
- [5] S. Zhang, N. Nishi, S. Katakura, T. Sakka, Evaluation of static differential capacitance at the [C₄mim⁺][TFSA⁻]/electrode interface using molecular dynamics simulation combined with electrochemical surface plasmon resonance measurements, *Phys. Chem. Chem. Phys.* 23 (2021) 13905–13917. <https://doi.org/10.1039/D1CP01435H>.
- [6] A. Uysal, H. Zhou, G. Feng, S.S. Lee, S. Li, P.T. Cummings, P.F. Fulvio, S. Dai, J.K. McDonough, Y. Gogotsi, P. Fenter, Interfacial ionic ‘liquids’: connecting static and dynamic structures, *J. Phys. Condens. Matter* 27 (2015) 032101. <https://doi.org/10.1088/0953-8984/27/3/032101>.
- [7] N. Nishi, J. Uchiyashiki, T. Oda, M. Hino, N.L. Yamada, Overscreening Induced by Ionic Adsorption at the Ionic Liquid/Electrode Interface Detected Using Neutron Reflectometry with a Rational Material Design, *Bull. Chem. Soc. Jpn.* 94 (2021) 2914–2918. <https://doi.org/10.1246/bcsj.20210328>.
- [8] T. Sieling, I. Brand, In Situ Spectroelectrochemical Investigation of Potential-Dependent Changes in an Amphiphilic Imidazolium-Based Ionic Liquid Film on the Au(111) Electrode Surface, *ChemElectroChem* 7 (2020) 3233–3243. <https://doi.org/10.1002/celec.202000385>.
- [9] A.C. Forse, C. Merlet, J.M. Griffin, C.P. Grey, New Perspectives on the Charging Mechanisms of Supercapacitors, *J. Am. Chem. Soc.* 138 (2016) 5731–5744. <https://doi.org/10.1021/jacs.6b02115>.
- [10] F. Greco, S. Shin, F.J. Williams, B.S.J. Heller, F. Maier, H.-P. Steinrück, Potential Screening at Electrode/Ionic Liquid Interfaces from In Situ X-ray Photoelectron Spectroscopy, *ChemistryOpen* 8 (2019) 1365–1368. <https://doi.org/10.1002/open.201900211>.
- [11] Y.-Z. Su, J.-W. Yan, M.-G. Li, Z.-X. Xie, B.-W. Mao, Z.-Q. Tian, Adsorption of Solvent Cations on Au(111) and Au(100) in Alkylimidazolium-Based Ionic Liquids - Worm-Like versus Micelle-Like Structures, *Z. Phys. Chem.-Int. J. Res.* 226 (2012) 979–994. <https://doi.org/10.1524/zpch.2012.0255>.
- [12] A.J. Page, A. Elbourne, R. Stefanovic, M.A. Addicoat, G.G. Warr, K. Voitchovsky, R. Atkin, 3-Dimensional atomic scale structure of the ionic liquid–graphite interface elucidated by AM-AFM and quantum chemical simulations, *Nanoscale* 6 (2014) 8100–8106. <https://doi.org/10.1039/C4NR01219D>.
- [13] A. Elbourne, S. McDonald, K. Voitchovsky, F. Endres, G.G. Warr, R. Atkin, Nanostructure of the Ionic Liquid–Graphite Stern Layer, *ACS Nano* 9 (2015) 7608–7620. <https://doi.org/10.1021/acsnano.5b02921>.
- [14] F. Buchner, K. Forster-Tonigold, B. Uhl, D. Alwast, N. Wagner, A. Groß, R.J. Behm, Towards the Microscopic Identification of Anions and Cations at the Ionic Liquid | Ag(111) Interface: A Combined Experimental and Theoretical Investigation, *ACS Nano* 7 (2013) 7773–7784.
- [15] J. Hoth, F. Hausen, M.H. Müser, R. Bennewitz, Force microscopy of layering and friction in an ionic liquid, *J. Phys. Condens. Matter* 26 (2014) 284110.

- <https://doi.org/10.1088/0953-8984/26/28/284110>.
- [16] R. Wen, B. Rahn, Olaf.M. Magnussen, In Situ Video-STM Study of Adlayer Structure and Surface Dynamics at the Ionic Liquid/Au (111) Interface, *J. Phys. Chem. C* 120 (2016) 15765–15771. <https://doi.org/10.1021/acs.jpcc.5b11590>.
- [17] M.-G. Li, L. Chen, Y.-X. Zhong, Z.-B. Chen, J.-W. Yan, B.-W. Mao, The electrochemical interface of Ag(111) in 1-ethyl-3-methylimidazolium bis(trifluoromethylsulfonyl)imide ionic liquid—A combined in-situ scanning probe microscopy and impedance study, *Electrochimica Acta* 197 (2016) 282–289. <https://doi.org/10.1016/j.electacta.2015.12.227>.
- [18] J. Wallauer, M. Drüscher, B. Huber, B. Roling, The Differential Capacitance of Ionic Liquid / Metal Electrode Interfaces – A Critical Comparison of Experimental Results with Theoretical Predictions, *Z. Für Naturforschung B* 68 (2013) 1143–1153. <https://doi.org/doi:10.5560/znb.2013-3153>.
- [19] Y. Su, J. Yan, M. Li, M. Zhang, B. Mao, Electric Double Layer of Au(100)/Imidazolium-Based Ionic Liquids Interface: Effect of Cation Size, *J. Phys. Chem. C* 117 (2013) 205–212. <https://doi.org/10.1021/jp3079919>.
- [20] C. Gomes, R. Costa, C.M. Pereira, A.F. Silva, The electrical double layer at the ionic liquid/Au and Pt electrode interface, *RSC Adv.* 4 (2014) 28914–28921. <https://doi.org/10.1039/C4RA03977G>.
- [21] R. Costa, I.V. Voroshylova, M.N.D.S. Cordeiro, C.M. Pereira, A.F. Silva, Enhancement of differential double layer capacitance and charge accumulation by tuning the composition of ionic liquids mixtures, *Electrochimica Acta* 261 (2018) 214–220. <https://doi.org/10.1016/j.electacta.2017.12.134>.
- [22] N. Zhang, X.-R. Wang, Y.-X. Yuan, H.-F. Wang, M.-M. Xu, Z.-G. Ren, J.-L. Yao, R.-A. Gu, Probing double layer structure at Au/[BMIm]BF₄ interface by molecular length-dependent SERS Stark effect, *J. Electroanal. Chem.* 751 (2015) 137–143. <https://doi.org/10.1016/j.jelechem.2015.05.041>.
- [23] L. Siinor, C. Siimenson, V. Ivaništšev, K. Lust, E. Lust, Influence of cation chemical composition and structure on the double layer capacitance for Bi(111) | room temperature ionic liquid interface, *J. Electroanal. Chem.* 668 (2012) 30–36. <https://doi.org/10.1016/j.jelechem.2012.01.005>.
- [24] T. Pajkossy, C. Müller, T. Jacob, The metal–ionic liquid interface as characterized by impedance spectroscopy and in situ scanning tunneling microscopy, *Phys. Chem. Chem. Phys.* 20 (2018) 21241–21250. <https://doi.org/10.1039/C8CP02074D>.
- [25] W. Dean, J. Klein, B. Gurkan, Do Deep Eutectic Solvents Behave Like Ionic Liquid Electrolytes? A Perspective from the Electrode-Electrolyte Interface, *J. Electrochem. Soc.* 168 (2021) 026503. <https://doi.org/10.1149/1945-7111/abde83>.
- [26] N. Hjalmarrsson, D. Wallinder, S. Glavatskih, R. Atkin, T. Aastrup, M.W. Rutland, Weighing the surface charge of an ionic liquid, *Nanoscale* 7 (2015) 16039–16045. <https://doi.org/10.1039/C5NR03965G>.
- [27] M. Schammer, A. Latz, B. Horstmann, The Role of Energy Scales for the Structure of Ionic Liquids at Electrified Interfaces: A Theory-Based Approach, *J. Phys. Chem. B* 126 (2022) 2761–2776. <https://doi.org/10.1021/acs.jpcc.2c00215>.
- [28] M.Z. Bazant, B.D. Storey, A.A. Kornyshev, Double Layer in Ionic Liquids: Overscreening versus Crowding, *Phys. Rev. Lett.* 106 (2011) 046102. <https://doi.org/10.1103/PhysRevLett.106.046102>.

- [29] J.P. de Souza, Z.A.H. Goodwin, M. McEldrew, A.A. Kornyshev, M.Z. Bazant, Interfacial Layering in the Electric Double Layer of Ionic Liquids, *Phys. Rev. Lett.* 125 (2020) 116001. <https://doi.org/10.1103/PhysRevLett.125.116001>.
- [30] N. Gavish, A. Yochelis, Theory of Phase Separation and Polarization for Pure Ionic Liquids, *J. Phys. Chem. Lett.* 7 (2016) 1121–1126. <https://doi.org/10.1021/acs.jpcllett.6b00370>.
- [31] M.V. Fedorov, A.A. Kornyshev, Towards understanding the structure and capacitance of electrical double layer in ionic liquids, *Electrochimica Acta* 53 (2008) 6835–6840. <https://doi.org/10.1016/j.electacta.2008.02.065>.
- [32] M.V. Fedorov, A.A. Kornyshev, Ionic Liquid Near a Charged Wall: Structure and Capacitance of Electrical Double Layer, *J. Phys. Chem. B* 112 (2008) 11868–11872. <https://doi.org/10.1021/jp803440q>.
- [33] S. Begić, F. Chen, E. Jónsson, M. Forsyth, Overscreening and crowding in electrochemical ionic liquid systems, *Phys. Rev. Mater.* 3 (2019) 095801. <https://doi.org/10.1103/PhysRevMaterials.3.095801>.
- [34] K. Kirchner, T. Kirchner, V. Ivaništšev, M.V. Fedorov, Electrical double layer in ionic liquids: Structural transitions from multilayer to monolayer structure at the interface, *Electrochimica Acta* 110 (2013) 762–771. <https://doi.org/10.1016/j.electacta.2013.05.049>.
- [35] V. Ivaništšev, S. O'Connor, M.V. Fedorov, Poly(a)morphic portrait of the electrical double layer in ionic liquids, *Electrochem. Commun.* 48 (2014) 61–64. <https://doi.org/10.1016/j.elecom.2014.08.014>.
- [36] I.V. Voroshylova, H. Ers, V. Koverga, B. Docampo-Álvarez, P. Pikma, V.B. Ivaništšev, M.N.D.S. Cordeiro, Ionic liquid–metal interface: The origins of capacitance peaks, *Electrochimica Acta* 379 (2021) 138148. <https://doi.org/10.1016/j.electacta.2021.138148>.
- [37] M. Giroto, A.M. Alencar, Modified 3D Ewald Summation for Slab Geometry at Constant Potential, *J. Phys. Chem. B* 124 (2020) 7842–7848. <https://doi.org/10.1021/acs.jpccb.0c03510>.
- [38] J.L. Ma, Q. Meng, J. Fan, Charge driven lateral structural evolution of ions in electric double layer capacitors strongly correlates with differential capacitance, *Phys. Chem. Chem. Phys.* 20 (2018) 8054–8063. <https://doi.org/10.1039/C7CP08075A>.
- [39] N. Georgi, A.A. Kornyshev, M.V. Fedorov, The anatomy of the double layer and capacitance in ionic liquids with anisotropic ions: Electrostriction vs. lattice saturation, *J. Electroanal. Chem.* 649 (2010) 261–267.
- [40] M. Belotti, X. Lyu, L. Xu, P. Halat, N. Darwish, D.S. Silvester, C. Goh, E.I. Izgorodina, M.L. Coote, S. Ciampi, Experimental Evidence of Long-Lived Electric Fields of Ionic Liquid Bilayers, *J. Am. Chem. Soc.* 143 (2021) 17431–17440. <https://doi.org/10.1021/jacs.1c06385>.
- [41] L.A. Jurado, R.M. Espinosa-Marzal, Insight into the Electrical Double Layer of an Ionic Liquid on Graphene, *Sci. Rep.* 7 (2017) 4225. <https://doi.org/10.1038/s41598-017-04576-x>.
- [42] T. Douglas, S. Yoo, P. Dutta, Ionic Liquid Solutions Show Anomalous Crowding Behavior at an Electrode Surface, *Langmuir* 38 (2022) 6322–6329. <https://doi.org/10.1021/acs.langmuir.2c00036>.

- [43] M. Chu, M. Miller, P. Dutta, Crowding and Anomalous Capacitance at an Electrode–Ionic Liquid Interface Observed Using Operando X-ray Scattering, *ACS Cent. Sci.* 2 (2016) 175–180. <https://doi.org/10.1021/acscentsci.6b00014>.
- [44] M. Chu, M. Miller, T. Douglas, P. Dutta, Ultraslow Dynamics at a Charged Silicon–Ionic Liquid Interface Revealed by X-ray Reflectivity, *J. Phys. Chem. C* 121 (2017) 3841–3845. <https://doi.org/10.1021/acs.jpcc.6b10443>.
- [45] J.M. Klein, H. Squire, B. Gurkan, Electroanalytical Investigation of the Electrode–Electrolyte Interface of Quaternary Ammonium Ionic Liquids: Impact of Alkyl Chain Length and Ether Functionality, *J. Phys. Chem. C* 124 (2020) 5613–5623. <https://doi.org/10.1021/acs.jpcc.9b08016>.
- [46] S. Zhang, T. Sakka, N. Nishi, Slow and Fast Dynamics at the Ionic Liquid/Gold Electrode Interface Separately Probed by Electrochemical Surface Plasmon Resonance Combined with Sequential Potential Pulse Techniques, *J. Electrochem. Soc.* 169 (2022) 066501. <https://doi.org/10.1149/1945-7111/ac58c4>.
- [47] S. Katakura, K. Amano, T. Sakka, W. Bu, B. Lin, M.L. Schlossman, N. Nishi, Evolution and Reversible Polarity of Multilayering at the Ionic Liquid/Water Interface, *J. Phys. Chem. B* 124 (2020) 6412–6419. <https://doi.org/10.1021/acs.jpcc.0c03711>.
- [48] S. Katakura, N. Nishi, K. Kobayashi, K. Amano, T. Sakka, Effect of Switching the Length of Alkyl Chains on Electric Double Layer Structure and Differential Capacitance at the Electrode Interface of Quaternary Ammonium-Based Ionic Liquids Studied Using Molecular Dynamics Simulation, *J. Phys. Chem. C* 124 (2020) 7873–7883. <https://doi.org/10.1021/acs.jpcc.0c00795>.
- [49] J. Ma, S. Zhao, Z. Li, New Crowding States of Ionic Liquid Induced by Configuration Change of Ion Adsorption on Charged Electrode, *SSRN Electron. J.* (2022). <https://doi.org/10.2139/ssrn.4072779>.
- [50] S.A. Kislenko, Yu.O. Moroz, K. Karu, V.B. Ivaništšev, M.V. Fedorov, Calculating the Maximum Density of the Surface Packing of Ions in Ionic Liquids, *Russ. J. Phys. Chem. A* 92 (2018) 999–1005. <https://doi.org/10.1134/S0036024418050187>.
- [51] R.M. Lynden-Bell, M.G. Del Pópolo, T.G.A. Youngs, J. Kohanoff, C.G. Hanke, J.B. Harper, C.C. Pinilla, Simulations of Ionic Liquids, Solutions, and Surfaces, *Acc. Chem. Res.* 40 (2007) 1138–1145. <https://doi.org/10.1021/ar700065s>.
- [52] C. Merlet, B. Rotenberg, P.A. Madden, M. Salanne, Computer simulations of ionic liquids at electrochemical interfaces, *Phys. Chem. Chem. Phys.* 15 (2013) 15781–15792.
- [53] J. Vatamanu, D. Bedrov, O. Borodin, On the application of constant electrode potential simulation techniques in atomistic modelling of electric double layers, *Mol. Simul.* 43 (2017) 838–849. <https://doi.org/10.1080/08927022.2017.1279287>.
- [54] L. Scalfi, M. Salanne, B. Rotenberg, Molecular Simulation of Electrode-Solution Interfaces, *Annu. Rev. Phys. Chem.* 72 (2021) 189–212. <https://doi.org/10.1146/annurev-physchem-090519-024042>.
- [55] T. Dufils, G. Jeanmairet, B. Rotenberg, M. Sprik, M. Salanne, Simulating Electrochemical Systems by Combining the Finite Field Method with a Constant Potential Electrode, *Phys. Rev. Lett.* 123 (2019) 195501. <https://doi.org/10.1103/PhysRevLett.123.195501>.
- [56] A. Groß, Structure of Electrode-Electrolyte Interfaces, Modeling of Double Layer

- and Electrode Potential, in: W. Andreoni, S. Yip (Eds.), *Handb. Mater. Model.*, Springer International Publishing, Cham, 2020: pp. 1439–1472.
https://doi.org/10.1007/978-3-319-44680-6_7.
- [57] W. Schmickler, E. Santos, *Interfacial electrochemistry*, 2nd ed., Springer, Heidelberg, 2010.
- [58] I.V. Voroshylova, M. Lembinen, H. Ers, M. Mišin, V.A. Koverga, C.M. Pereira, V.B. Ivaniššev, M.N.D.S. Cordeiro, On the role of the surface charge plane position at Au(*hkl*)–BMImPF₆ interfaces, *Electrochimica Acta* 318 (2019) 76–82.
<https://doi.org/10.1016/j.electacta.2019.05.058>.
- [59] C. Schröder, Comparing reduced partial charge models with polarizable simulations of ionic liquids, *Phys. Chem. Chem. Phys.* 14 (2012) 3089–3102.
<https://doi.org/10.1039/C2CP23329K>.
- [60] N.D. Lang, W. Kohn, Theory of Metal Surfaces: Induced Surface Charge and Image Potential, *Phys. Rev. B* 7 (1973) 3541–3550.
<https://doi.org/10.1103/physrevb.7.3541>.
- [61] N.D. Lang, W. Kohn, Theory of Metal Surfaces: Work Function, *Phys. Rev. B* 3 (1971) 1215–1223. <https://doi.org/10.1103/PhysRevB.3.1215>.
- [62] N.B. Luque, W. Schmickler, The electric double layer on graphite, *Electrochimica Acta* 71 (2012) 82–85. <https://doi.org/10.1016/j.electacta.2012.03.083>.
- [63] A.A. Kornyshev, N.B. Luque, W. Schmickler, Differential capacitance of ionic liquid interface with graphite: the story of two double layers, *J. Solid State Electrochem.* 18 (2014) 1345–1349.
- [64] E. Roos Nerut, K. Karu, I.V. Voroshylova, K. Kirchner, T. Kirchner, M.V. Fedorov, V.B. Ivaniššev, NaRIBaS—A Scripting Framework for Computational Modeling of Nanomaterials and Room Temperature Ionic Liquids in Bulk and Slab, *Computation* 6 (2018) 57. <https://doi.org/10.3390/computation6040057>.
- [65] J.N. Canongia Lopes, J. Deschamps, A.A.H. Pádua, Modeling Ionic Liquids Using a Systematic All-Atom Force Field, *J. Phys. Chem. B* 108 (2004) 2038–2047.
<https://doi.org/10.1021/jp0362133>.
- [66] J.N. Canongia Lopes, J. Deschamps, A.A.H. Pádua, Modeling Ionic Liquids Using a Systematic All-Atom Force Field, *J. Phys. Chem. B* 108 (2004) 11250–11250.
<https://doi.org/10.1021/jp0476996>.
- [67] J.N. Canongia Lopes, A.A.H. Pádua, K. Shimizu, Molecular Force Field for Ionic Liquids IV: Trialkylimidazolium and Alkoxy carbonyl-Imidazolium Cations; Alkylsulfonate and Alkylsulfate Anions, *J. Phys. Chem. B* 112 (2008) 5039–5046.
<https://doi.org/10.1021/jp800281e>.
- [68] A.H. Larsen, J.J. Mortensen, J. Blomqvist, I.E. Castelli, R. Christensen, M. Dulak, J. Friis, M.N. Groves, B. Hammer, C. Hargus, E.D. Hermes, P.C. Jennings, P.B. Jensen, J. Kermode, J.R. Kitchin, E.L. Kolsbjerg, J. Kubal, K. Kaasbjerg, S. Lysgaard, J.B. Maronsson, T. Maxson, T. Olsen, L. Pastewka, A. Peterson, C. Rostgaard, J. Schiøtz, O. Schütt, M. Strange, K.S. Thygesen, T. Vegge, L. Vilhelmsen, M. Walter, Z. Zeng, K.W. Jacobsen, The atomic simulation environment—a Python library for working with atoms, *J. Phys. Condens. Matter* 29 (2017) 273002.
<https://doi.org/10.1088/1361-648X/aa680e>.
- [69] L. Martínez, R. Andrade, E.G. Birgin, J.M. Martínez, PACKMOL: A Package for Building Initial Configurations for Molecular Dynamics Simulations, *J. Comput.*

- Chem. 30 (2009) 2157–2164. <https://doi.org/10.1002/jcc.21224>.
- [70] O.M. Magnussen, Ordered Anion Adlayers on Metal Electrode Surfaces, *Chem. Rev.* 102 (2002) 679–726. <https://doi.org/10.1021/cr000069p>.
- [71] C. Noh, Y. Jung, Understanding the charging dynamics of an ionic liquid electric double layer capacitor via molecular dynamics simulations, *Phys. Chem. Chem. Phys.* 21 (2019) 6790–6800. <https://doi.org/10.1039/C8CP07200K>.
- [72] F. Tang, T. Ohto, T. Hasegawa, M. Bonn, Y. Nagata, $\pi^+-\pi^+$ stacking of imidazolium cations enhances molecular layering of room temperature ionic liquids at their interfaces, *Phys Chem Chem Phys* 19 (2017) 2850–2856. <https://doi.org/10.1039/C6CP07034E>.
- [73] A.J.L. Costa, M.R.C. Soromenho, K. Shimizu, I.M. Marrucho, J.M.S.S. Esperança, J.N.C. Lopes, L.P.N. Rebelo, Density, Thermal Expansion and Viscosity of Cholinium-Derived Ionic Liquids, *ChemPhysChem* 13 (2012) 1902–1909. <https://doi.org/10.1002/cphc.201100852>.
- [74] M. Součková, J. Klomfar, J. Pátek, Surface tension and 0.1 MPa densities of imidazolium-, pyridinium-, pyrrolidinium-, and piperidinium-based tris(pentafluoroethyl)trifluorophosphate ionic liquids, *Fluid Phase Equilibria* 333 (2012) 38–46. <https://doi.org/10.1016/j.fluid.2012.07.013>.
- [75] W. Humphrey, A. Dalke, K. Schulten, VMD: Visual molecular dynamics, *J. Mol. Graph.* 14 (1996) 33–38. [https://doi.org/10.1016/0263-7855\(96\)00018-5](https://doi.org/10.1016/0263-7855(96)00018-5).
- [76] S. Grimme, A. Hansen, S. Ehlert, J.-M. Mewes, r^2 SCAN-3c: A “Swiss army knife” composite electronic-structure method, *J. Chem. Phys.* 154 (2021) 064103. <https://doi.org/10.1063/5.0040021>.
- [77] F. Neese, F. Wennmohs, U. Becker, C. Riplinger, The ORCA quantum chemistry program package, *J. Chem. Phys.* 152 (2020) 224108. <https://doi.org/10.1063/5.0004608>.
- [78] O. Oll, C. Siimenson, K. Lust, G. Gorbatovski, E. Lust, Specific adsorption from an ionic liquid: impedance study of iodide ion adsorption from a pure halide ionic liquid at bismuth single crystal planes, *Electrochimica Acta* 247 (2017) 910–919. <https://doi.org/10.1016/j.electacta.2017.07.034>.
- [79] X. Zhang, Y.-X. Zhong, J.-W. Yan, Y.-Z. Su, M. Zhang, B.-W. Mao, Probing double layer structures of Au (111)–BMIPF 6 ionic liquid interfaces from potential-dependent AFM force curves, *Chem. Commun.* 48 (2012) 582–584. <https://doi.org/10.1039/C1CC15463J>.
- [80] E. Anderson, V. Grozovski, L. Siinor, C. Siimenson, E. Lust, In situ STM studies of Bi(111)|1-ethyl-3-methylimidazolium tetrafluoroborate + 1-ethyl-3-methylimidazolium iodide interface, *Electrochem. Commun.* 46 (2014) 18–21. <https://doi.org/10.1016/j.elecom.2014.05.032>.
- [81] R. Wen, B. Rahn, O.M. Magnussen, Potential-Dependent Adlayer Structure and Dynamics at the Ionic Liquid/Au(111) Interface: A Molecular-Scale In Situ Video-STM Study, *Angew. Chem. Int. Ed.* 54 (2015) 6062–6066. <https://doi.org/10.1002/anie.201501715>.
- [82] H. Kruse, S. Grimme, A geometrical correction for the inter- and intra-molecular basis set superposition error in Hartree-Fock and density functional theory calculations for large systems, *J. Chem. Phys.* 136 (2012) 154101. <https://doi.org/10.1063/1.3700154>.

- [83] Y. Fu, A.V. Rudnev, Scanning probe microscopy of an electrode/ionic liquid interface, *Curr. Opin. Electrochem.* 1 (2017) 59–65. <https://doi.org/10.1016/j.coelec.2017.01.005>.
- [84] V. Ivaništšev, Repository for: NaRIBaS—A Scripting Framework for Computational Modeling of Nanomaterials and Room Temperature Ionic Liquids in Bulk and Slab, GitHub Repos. (2018). <https://github.com/vilab-tartu/NaRIBaS>.
- [85] V. Ivaništšev, Gromacs topology files for common Ionic Liquids, GitHub Repos. (2018). <https://doi.org/10.5281/zenodo.1435766>.
- [86] I.V. Voroshlyova, H. Ers, B. Docampo-Álvarez, P. Pikma, V.B. Ivaništšev, M.N.D.S. Cordeiro, Hysteresis in the MD Simulations of Differential Capacitance at the Ionic Liquid–Au Interface, *J. Phys. Chem. Lett.* 11 (2020) 10408–10413. <https://doi.org/10.1021/acs.jpcclett.0c03212>.
- [87] S. Baldelli, Surface Structure at the Ionic Liquid–Electrified Metal Interface, *Acc. Chem. Res.* 41 (2008) 421–431. <https://doi.org/10.1021/ar700185h>.
- [88] Z. Dai, Y. You, Y. Zhu, S. Wang, W. Zhu, X. Lu, Atomistic Insights into the Layered Microstructure and Time-Dependent Stability of [BMIM][PF6] Confined within the Meso-Slit of Carbon, *J. Phys. Chem. B* 123 (2019) 6857–6869. <https://doi.org/10.1021/acs.jpcc.9b02682>.
- [89] E.S.C. Ferreira, C.M. Pereira, M.N.D.S. Cordeiro, D.J.V.A. dos Santos, Molecular Dynamics Study of the Gold/Ionic Liquids Interface, *J. Phys. Chem. B* 119 (2015) 9883–9892. <https://doi.org/10.1021/acs.jpcc.5b04505>.
- [90] K. Zhang, G. Zhou, T. Fang, X. Tang, X. Liu, Surface-active ionic liquids near the electrode surface: Development and influence on molecular dynamics simulations, *Appl. Surf. Sci.* 614 (2023) 156200. <https://doi.org/10.1016/j.apsusc.2022.156200>.
- [91] A.M. Smith, K.R.J. Lovelock, N.N. Gosvami, P. Licence, A. Dolan, T. Welton, S. Perkin, Monolayer to Bilayer Structural Transition in Confined Pyrrolidinium-Based Ionic Liquids, *J. Phys. Chem. Lett.* 4 (2013) 378–382. <https://doi.org/10.1021/jz301965d>.
- [92] S. Perkin, L. Crowhurst, H. Niedermeyer, T. Welton, A.M. Smith, N.N. Gosvami, Self-assembly in the electrical double layer of ionic liquids, *Chem. Commun.* 47 (2011) 6572–6574. <https://doi.org/10.1039/C1CC11322D>.
- [93] S. Watanabe, G.A. Pilkington, A. Oleshkevych, P. Pedraz, M. Radiom, R. Welbourn, S. Glavatskih, M.W. Rutland, Interfacial structuring of non-halogenated imidazolium ionic liquids at charged surfaces: effect of alkyl chain length, *Phys. Chem. Chem. Phys.* 22 (2020) 8450–8460. <https://doi.org/10.1039/D0CP00360C>.
- [94] S. Sharma, H.K. Kashyap, Structure of Quaternary Ammonium Ionic Liquids at Interfaces: Effects of Cation Tail Modification with Isoelectronic Groups, *J. Phys. Chem. C* 119 (2015) 23955–23967. <https://doi.org/10.1021/acs.jpcc.5b06460>.
- [95] V. Ivaništšev, M.V. Fedorov, Interfaces between Charged Surfaces and Ionic Liquids: Insights from Molecular Simulations, *Electrochem. Soc. Interface* 23 (2014) 65–69. <https://doi.org/10.1149/2.F08141if>.
- [96] W.M. Haynes, D.R. Lide, T.J. Bruno, *CRC handbook of chemistry and physics*, CRC press Boca Raton, FL, 2017.
- [97] E. Anderson, V. Grozovski, L. Siinor, C. Siimenson, V. Ivaništšev, K. Lust, S. Kallip, E. Lust, Influence of the electrode potential and in situ STM scanning conditions on the phase boundary structure of the single crystal

- Bi(1 1 1)|1-butyl-4-methylpyridinium tetrafluoroborate interface, *J. Electroanal. Chem.* 709 (2013) 46–56. <https://doi.org/10.1016/j.jelechem.2013.10.004>.
- [98] O. Oll, M. Väärtnõu, G. Gorbatovski, J. Zhao, C. Siimenson, L. Siinor, K. Lust, T. Romann, P. Pikma, E. Lust, Adsorption of anions on bismuth and cadmium single crystal plane electrodes from various solvents and ionic liquid mixtures, *Electrochimica Acta* 319 (2019) 895–908. <https://doi.org/10.1016/j.electacta.2019.06.179>.
- [99] L. Siinor, H. Ers, P. Pikma, Another Piece of the Ionic Liquid’s Puzzle: Adsorption of Cl⁻ Ions, *J. Phys. Chem. C* 128 (2024) 2722–2729. <https://doi.org/10.1021/acs.jpcc.3c07991>.
- [100] S. Snegir, Y.J. Dappe, D. Sysoiev, O. Pluchery, T. Huhn, E. Scheer, Where do the counterions go? Tip-induced dissociation of self-assembled triazatriangulenium-based molecules on Au(111), *Phys. Chem. Chem. Phys.* 23 (2021) 9930–9937. <https://doi.org/10.1039/D1CP00221J>.
- [101] G.-B. Pan, W. Freyland, 2D phase transition of PF₆ adlayers at the electrified ionic liquid/Au(111) interface, *Chem. Phys. Lett.* 427 (2006) 96–100. <https://doi.org/10.1016/j.cplett.2006.05.114>.
- [102] R. Atkin, N. Borisenko, M. Drüschler, S.Z. El Abedin, F. Endres, R. Hayes, B. Huber, B. Roling, An in situ STM/AFM and impedance spectroscopy study of the extremely pure 1-butyl-1-methylpyrrolidinium tris(pentafluoroethyl)trifluorophosphate/Au(111) interface: potential dependent solvation layers and the herringbone reconstruction, *Phys. Chem. Chem. Phys.* 13 (2011) 6849–6857. <https://doi.org/10.1039/c0cp02846k>.
- [103] N. Borisenko, S.Z. El Abedin, F. Endres, An in Situ STM and DTS Study of the Extremely Pure [EMIM]FAP/Au(111) Interface, *Chemphyschem* 13 (2012) 1736–1742. <https://doi.org/10.1002/cphc.201100873>.
- [104] W.-Y. Tsai, J. Come, W. Zhao, R. Wang, G. Feng, B. Prasad Thapaliya, S. Dai, L. Collins, N. Balke, Hysteretic order-disorder transitions of ionic liquid double layer structure on graphite, *Nano Energy* 60 (2019) 886–893. <https://doi.org/10.1016/j.nanoen.2019.04.022>.
- [105] S. Kondrat, G. Feng, F. Bresme, M. Urbakh, A.A. Kornyshev, Theory and Simulations of Ionic Liquids in Nanoconfinement, *Chem. Rev.* 123 (2023) 6668–6715. <https://doi.org/10.1021/acs.chemrev.2c00728>.
- [106] M.V. Fedorov, A.A. Kornyshev, Ionic Liquids at Electrified Interfaces, *Chem. Rev.* 114 (2014) 2978–3036. <https://doi.org/10.1021/cr400374x>.
- [107] J. Wu, Understanding the Electric Double-Layer Structure, Capacitance, and Charging Dynamics, *Chem. Rev.* 122 (2022) 10821–10859. <https://doi.org/10.1021/acs.chemrev.2c00097>.
- [108] H. Ers, I.V. Voroshylova, P. Pikma, V.B. Ivaništšev, Double layer in ionic liquids: Temperature effect and bilayer model, *J. Mol. Liq.* 363 (2022) 119747. <https://doi.org/10.1016/j.molliq.2022.119747>.
- [109] I. Borukhov, D. Andelman, H. Orland, Adsorption of large ions from an electrolyte solution: a modified Poisson–Boltzmann equation, *Electrochimica Acta* 46 (2000) 221–229. [https://doi.org/10.1016/S0013-4686\(00\)00576-4](https://doi.org/10.1016/S0013-4686(00)00576-4).
- [110] I. Borukhov, D. Andelman, H. Orland, Steric Effects in Electrolytes: A Modified Poisson-Boltzmann Equation, *Phys. Rev. Lett.* 79 (1997) 435–438.

- <https://doi.org/10.1103/PhysRevLett.79.435>.
- [111] D.M. Hudgins, Jr. Charles W. Bauschlicher, L.J. Allamandola, Variations in the Peak Position of the 6.2 μm Interstellar Emission Feature: A Tracer of N in the Interstellar Polycyclic Aromatic Hydrocarbon Population, *Astrophys. J.* 632 (2005) 316–332. <https://doi.org/10.1086/432495>.
- [112] L.-F. Velázquez-López, S.-M. Pacheco-Ortín, R. Mejía-Olvera, E. Agacino-Valdés, DFT study of CO adsorption on nitrogen/boron doped-graphene for sensor applications, *J. Mol. Model.* 25 (2019) 91. <https://doi.org/10.1007/s00894-019-3973-z>.
- [113] S. Lemke, S. Ulrich, F. Claußen, A. Bloedorn, U. Jung, R. Herges, O.M. Magnussen, Triazatriangulenium adlayers on Au(111): Superstructure as a function of alkyl side chain length, *Surf. Sci.* 632 (2015) 71–76. <https://doi.org/10.1016/j.susc.2014.08.028>.
- [114] S. Ulrich, U. Jung, T. Strunskus, C. Schütt, A. Bloedorn, S. Lemke, E. Ludwig, L. Kipp, F. Faupel, O. Magnussen, R. Herges, X-ray spectroscopy characterization of azobenzene-functionalized triazatriangulenium adlayers on Au(111) surfaces, *Phys. Chem. Chem. Phys.* 17 (2015) 17053–17062. <https://doi.org/10.1039/C5CP01447F>.
- [115] H. Ers, R. Cepitis, V.B. Ivaništšev, Potential of monolayer charge, (2023). <https://doi.org/10.48550/arXiv.2301.13681>.
- [116] M.Z. Bazant, M.S. Kilic, B.D. Storey, A. Ajdari, Towards an understanding of induced-charge electrokinetics at large applied voltages in concentrated solutions, *Adv. Colloid Interface Sci.* 152 (2009) 48–88. <https://doi.org/10.1016/j.cis.2009.10.001>.